Available online at www.sciencedirect.com
SCIENCE DIRECT®
Journal of Catalysis 224 (2004) 197–205
JOURNAL OF CATALYSIS
www.elsevier.com/locate/jcat

Growing mechanism of CNTs: a kinetic approach

M. Pérez-Cabero,[a] E. Romeo,[b] C. Royo,[b] A. Monzón,[b,*] A. Guerrero-Ruíz,[c] and I. Rodríguez-Ramos [a,*]

[a] *Instituto de Catálisis y Petroleoquímica, CSIC, Marie Curie s/n, 28049 Cantoblanco, Madrid, Spain*
[b] *Departamento de Ingeniería Química y Tecnologías del Medio Ambiente, Facultad de Ciencias, Universidad de Zaragoza, Pedro Cerbuna 12, 50009 Zaragoza, Spain*
[c] *Departamento de Química Inorgánica y Técnica, Facultad de Ciencias, UNED, Senda del Rey 9, 28040 Madrid, Spain*

Received 11 December 2003; revised 2 March 2004; accepted 4 March 2004

Abstract

A kinetic study of the synthesis of carbon nanotubes (CNTs) by catalytic decomposition of acetylene over an iron-supported catalyst was carried out using a thermobalance. The CNTs were mainly characterized by transmission electron microscopy (TEM and HRTEM). It was found that there is a high influence of the reaction conditions (feed mixture, reaction temperature, etc.) on the final reaction yield and on the structural and morphological characteristics of the carbon products obtained. A complete discussion of the results by comparison of the carbon deposition curves with the TEM images is given. Finally, a kinetic model for explaining the growing mechanism of carbon nanotubes is developed and the displayed conclusions are clearly shown.

Keywords: Carbon nanotubes (CNTs); Carbon nanofibers (CNFs); Acetylene decomposition; CVD; Iron catalysts; Kinetic modeling; Catalyst deactivation

1. Introduction

The decomposition of several hydrocarbons over metallic surfaces has attracted the interest of many authors in the last century. For decades the formation of carbon filaments over metallic catalysts used in the conversion of carbon-containing gases (e.g., steam-methane-reforming reaction) has been reported as a serious problem due to the complete deactivation of the catalyst and possible damages in the reactor walls [1,2]. From the 1980s a few applications were found for these carbon filaments, but the first studies about their synthesis were in order to avoid their formation during the above-noted reactions [3]. However, it was not until 1991, when carbon nanotubes (CNTs) were discovered by Ijima [4], that interest in the formation of these species grew, in order to explore their novel and attractive properties [5,6].

The main problem of CNTs is the scalability and reproducibility of the synthesis, and consequently the full potential of CNTs for applications will not be realized until their growth can be further optimized and controlled. Among other factors, their future use will strongly depend on the development of simple, efficient, and inexpensive technologies for a large-scale production [7]. Several synthetic methods have been reported in the bibliography, such as arc discharch [8], laser ablation [9], or chemical vapor deposition (CVD) of hydrocarbon gases over a catalytic material [10]. The CVD method has been reported to be the most selective in the carbon nanotube formation [11]. It has been found that the structure of carbon materials is dependent on the growth parameters such as reaction temperature, catalyst, and reaction gases [12–15]. However, there are not many systematic studies on the influence of these parameters on the growth of CNTs using the CVD method [16].

Conditions for carbon deposition from acetylene on nickel catalysts are perhaps the topic most studied for the synthesis of CNTs [17–20]; however, most papers have covered the morphological aspects and so, information about the kinetics of the process has been scarce. With iron catalysts the available data in the bibliography are even less, although CNTs were easier to grow over Fe than over Co or Ni catalysts [21]. It seems that iron catalysts have an apparently less structure-sensitive interaction between formed carbon and metal particles than with nickel or cobalt; however, also

* Corresponding authors.
E-mail addresses: amonzon@posta.unizar.es (A. Monzón), irodriguez@icp.csic.es (I. Rodríguez-Ramos).

0021-9517/$ – see front matter
doi:10.1016/j.jcat.2004.03.003

in this case, kinetic studies of the synthesis of CNTs with iron catalysts are almost nonexistent.

The growth of carbon nanofibers by the CVD method is probably the most controversial since the first theories were proposed in the 1970s [22]. Nowadays it is mostly assumed that the first step is decomposition of the carbon source on the active points of the catalyst, giving carbon atoms with a concomitant desorption of molecular hydrogen. This carbon then dissolves and diffuses through the bulk of the metal, by the formation of an intermediate carbide species, which decomposes and regenerates the metal particle. This is the nucleation step of the process, which allows the growth of carbon filaments. From several magnetization measurements it appeared that a high carbide content is required before nucleation of carbon in the procedure [23]. The latter authors admit that the formation of this carbide species explains the thermodynamics of diffusion in the general mechanism [24–26]. Recently, using a pulse reaction method, it was shown that CNT formation occurs from the beginning of the acetylene decomposition reaction [27]. Thus the CNT growth rate seems to be faster than that of the nucleation step. Snoeck et al. [24] have proposed that the global driving force for carbon filament formation is the difference in chemical potential between the gas phase and the carbon filament. A carbon concentration gradient is thus created and it acts as the driving force for the diffusion process. The growing process of the carbon filaments can be blocked by encapsulation with carbon of the metal particles of the catalyst, and this will decrease the synthesis or even completely stop the process by deactivation of the catalyst [3,16]. Thus, in summary, we should expect three main steps: nucleation, growth and deactivation of the catalyst.

In this paper carbon nanotubes have been synthesized by the catalytic decomposition of acetylene, over an iron-supported catalyst in a thermobalance, which allows continuous control of the CNT synthesis in real time, under several reaction conditions. Our objective was to test, in a series of experiments, the growth mechanism of the CNTs under different reaction conditions. A complete kinetic study is achieved and a final mathematic model is developed. A good correlation is seen between the kinetic parameters described in this paper and the morphological properties of the carbon products isolated and studied by TEM.

2. Experimental and methods

The Fe/silica catalyst was prepared by impregnation in a rotatory evaporator. The iron precursor employed was $Fe(CO)_5$. A commercial silica gel (480 m^2/g), from Fluka, was used as support. An amount of 50 g of silica was mixed with 500 ml of an ethanolic solution of the metal complex (in the exact amount to get the required iron percentage of 1 wt%). The final solution was evaporated at 40 °C and 150 rpm under vacuum until the solid was dried. The catalyst was used in the reaction as prepared, thus without further calcinations, to avoid structure modifications or iron oxidation from the carbonyl complex.

The iron content for the prepared catalyst was analyzed in an atomic emission spectroscope (ICP) (Perkin-Elmer Model 3300 DV).

Temperature-programmed reduction (TPR) experiments were carried in a thermobalance (C.I. Electronic) with a small quartz basket where several milligrams of the samples was deposited. The reduction ran in a mixture of H_2/He (1/1), with a total gas flow rate of 20 ml/min, till 800 °C at approximately 5 °C/min. Blank experiments with the SiO_2 were also carried out.

Carbon nanotubes were synthesized by the catalytic decomposition of acetylene, over the iron catalyst previously described, in a thermobalance. The experimental system was the same as that used for the TPR experiments described above. Approximately 100 mg of the catalyst was deposited in the quartz basket. The reaction conditions, acetylene/hydrogen ratios and temperature, were modified in order to test the influence of the different parameters in the reaction yield. The catalyst was heated, in a mixture N_2/H_2 (100/100 ml/min), from room temperature to reaction temperature, with a heating ramp of 10 °C/min. After 120 min more at this temperature, acetylene was introduced in a reaction mixture of $N_2/C_2H_2/H_2$ (total flow rate of 500 ml/min) for 120 min. After this time the reactor was cooled to room temperature in a N_2 atmosphere.

The first series of experiments were carried out in order to determine the acetylene and hydrogen ratios to get the highest yield in carbon at 700 °C. Another series of experiments consisted in testing reaction temperatures from 600 to 800 °C using a fixed gas mixture in the reaction.

The products were characterized by transmission electron microscopy (TEM and HRTEM). The TEM studies were carried out in a JEOL JEM-2000 FX microscope at 200 kV and HRTEM studies in a JEOL JEM-4000 EX microscope at 400 kV. The samples were prepared by grinding and ultrasonic dispersal in an acetone solution, placed on the copper TEM grid, and evaporated.

3. Results and discussion

The catalyst employed for the reaction exhibited an iron content (1.09 wt%) in agreement with the theoretical statement. The TPR experiment, not shown for the sake of brevity, displayed a 13 wt% weight loss between room temperature and 200 °C, due to solvent or water desorption. The catalyst suffered a weight loss (2.1 wt%) between 200 and 600 °C that fits well with the decarbonylation of the iron precursor complex. Furthermore, we have studied by TEM the particle-size distribution of the samples reduced at 600 and 800 °C. We have not observed significant changes due to sintering of the metal particles in the surface of the catalyst with this increment of the reduction temperature. Then, we can admit that the metallic surface area of this catalyst remains

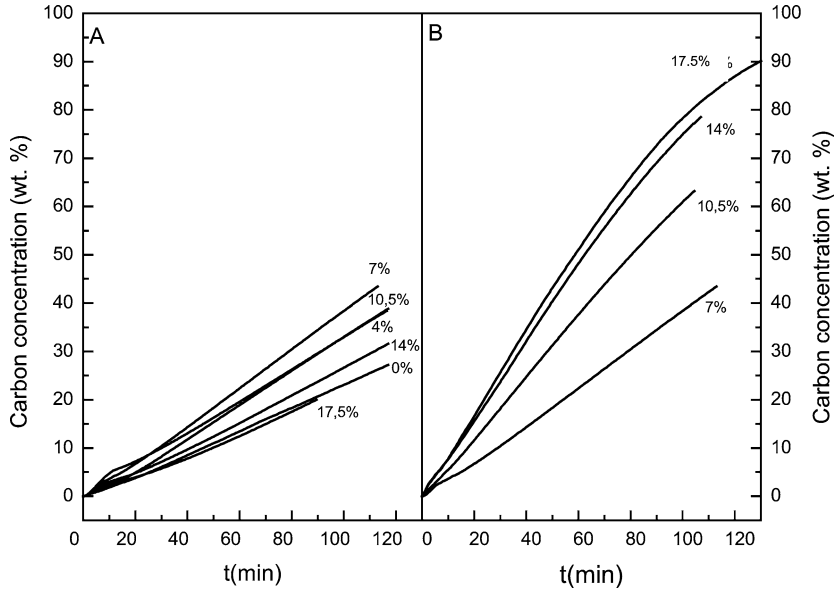

Fig. 1. (A) Influence of P_{H_2} in the synthesis of CNTs at 700 °C in a reaction mixture of $P_{C_2H_2}$ of 7% in N_2. (B) Influence of $P_{C_2H_2}$ in the synthesis of CNTs at 700 °C in a reaction mixture of P_{H_2} of 7% in N_2.

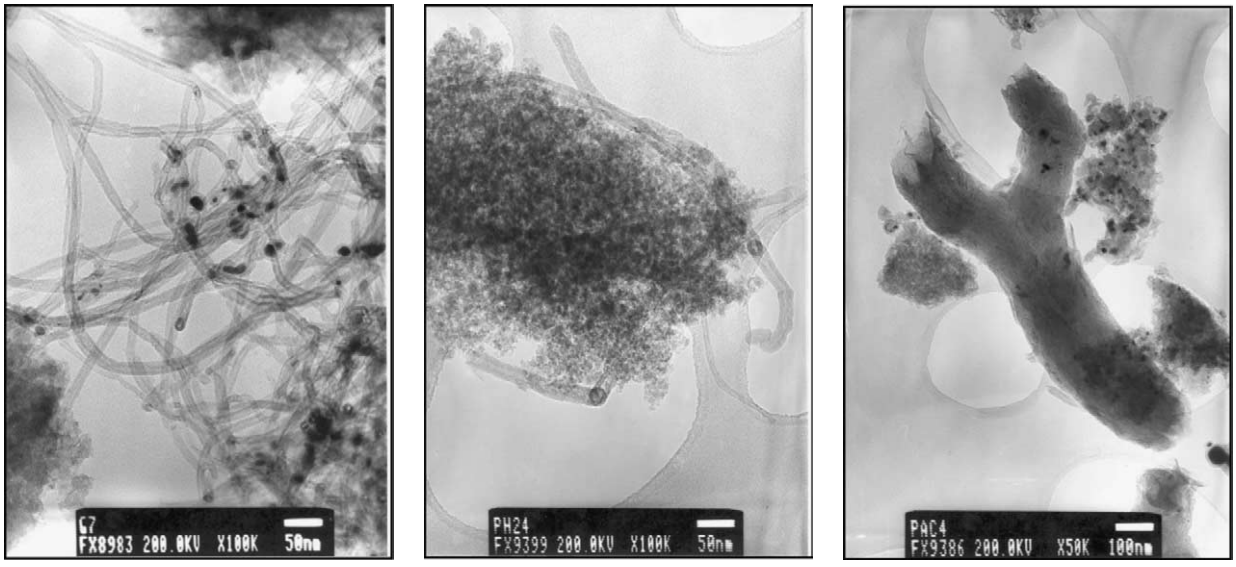

(a) (b) (c)

Fig. 2. TEM images of carbonaceous products at 700 °C under different gas mixtures: (a) CNTs obtained at $P_{H_2} = P_{C_2H_2} = 7\%$ in N_2, (b) CNTs obtained at $P_{H_2} = 17.5\%$, (c) CNFs obtained at $P_{C_2H_2} = 17.5\%$.

invariable in this range of temperatures, corresponding to an average particle size of approximately 8 nm.

The total amount of carbon deposited on the iron–silica catalyst after reaction was determined by weight gain in the thermobalance during reaction. The qualitative analysis of these samples was carried out by TEM and HRTEM. In Fig. 1A the influence of the hydrogen partial pressure (P_{H_2}) on carbon deposition at 700 °C in an acetylene gas mixture of 7% v/v in N_2 is seen. Although large differences among the distinct hydrogen:acetylene ratios were not observed, the hydrogen mixture of 7% v/v in N_2 (hydrogen:acetylene, 1:1) gave the highest yield in carbon products at 700 °C. TEM studies did not show high morphological differences in the carbon products synthesized under these P_{H_2} variations (see Figs. 2a and 2b). In all cases CNTs were mostly observed. The existence of this maximum in CNTs rate production can be justified because hydrogen probably acts in a double direction in this reaction. At low partial pressures it will mostly clean the catalyst surface, avoiding deactivation due to metal encapsulation. At high partial pressure this is in higher proportion, and it can react in a competitive way in acetylene hydrogenation. Thus, a decrease in the reaction yield is expected [16,28–30]. In Fig. 1B the influence of acetylene partial pressure ($P_{C_2H_2}$) in carbon deposition at

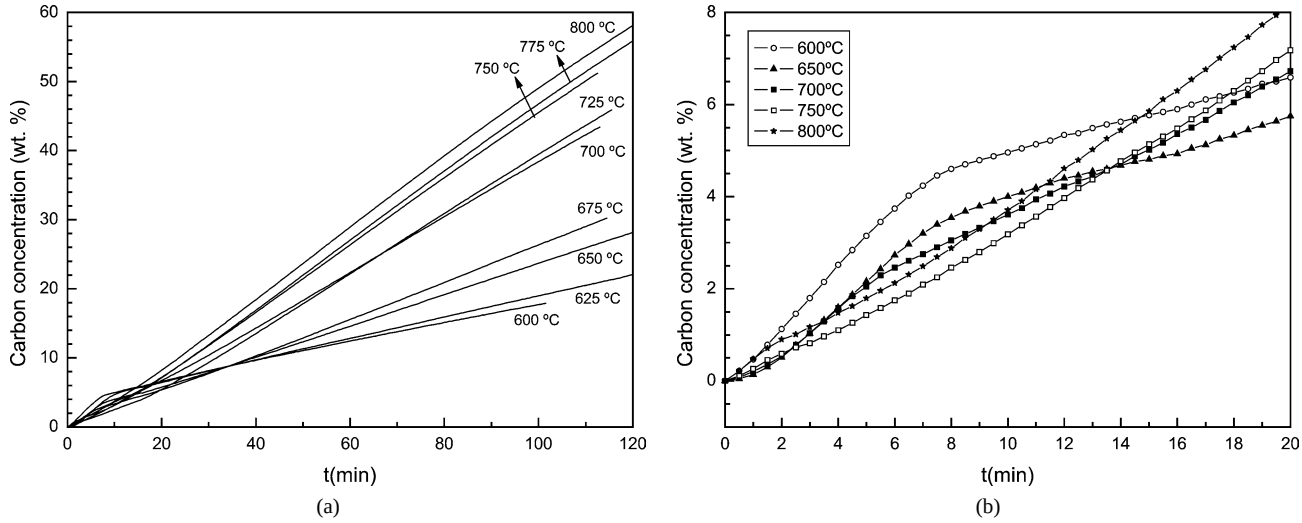

Fig. 3. Influence of reaction temperature in the synthesis of CNTs in a reaction mixture of $P_{H_2} = P_{C_2H_2} = 7\%$ in N_2: (a) all the reaction time, (b) initial growing period.

700 °C in a hydrogen reaction mixture of 7% v/v in N_2 is seen. It was observed that carbon yield was higher with the increase of $P_{C_2H_2}$, although the graphics showed a partial deactivation of the catalyst at high acetylene partial pressures, which is inferred from the final curvature of these profiles. In addition, TEM images revealed that the carbonaceous products became more heterogeneous with an increase of acetylene in the reaction mixture (see Figs. 2a and 2c). At $P_{C_2H_2}$ of 17.5% v/v in N_2 a high proportion of CNFs and carbon encapsulation of the metal particles was found, which confirmed the catalyst deactivation observed in the curves (Fig. 2c).

For the experiments at different reaction temperatures a reaction mixture of acetylene:hydrogen (1:1), in a partial pressure of 7% each in N_2 was chosen. Under these conditions a high yield of CNTs is produced, and at the same time, the catalyst deactivation is slow enough to allow us to follow the carbon deposit formations for several hours, in comparison with experiments with an excess of acetylene. In Fig. 3a the reaction results at temperatures from 600 to 800 °C with differences of 25 °C are seen. A direct relationship between temperature and carbon yield in this reaction was observed. At 800 °C almost a 60 wt% in carbon products was obtained. At first sight all the curves seem to have the same characteristics, but if we expand the first 20 min of the reaction, we can detect another important difference. In Fig. 3b we can observe how the reaction at 600 °C showed a quick carbon weight increase from minute 0, but after approximately 10 min the curve slope decreased, indicating a possible partial deactivation of the catalyst. We cannot speak about a total deactivation at this temperature because a carbon weight gain in at 2 h of the reaction was observed. At 650 °C the behavior is similar to that at 600 °C, but from 700 °C we observed important changes in the kinetics. From 700 up to 800 °C a linear weight increase was observed, without catalyst deactivation at 2 h of the reaction. TEM analysis corroborates these hypotheses, so that we observed rather amorphous carbon species at a low-temperature reaction up to 650 °C (see Fig. 4a), which caused the encapsulation of the catalyst metal particles. At higher temperatures, from 700 °C, we could observe a high proportion in CNTs, homogeneous in size and well graphitized, as also confirmed by HRTEM (see Figs. 4b and 4c).

Several papers have already dealt with the influence of temperature on the carbon products, but we decided to take further step and use the thermobalance data to apply a mathematic model to study the influence of the operating conditions on the CNT formation rate (A. Monzón et al., in preparation). The proposed model takes into account both stages of carbon formation, nucleation and CNT growth.

The mechanism of carbon filament formation assumes that the carbon atoms, formed on the metallic surface from the hydrocarbon decomposition, will react forming surface metallic carbide. The process of decomposition-segregation of this carbide allows the carbon atoms to penetrate into the metallic particle, and finally regenerate the metallic surface [24]. The evolution of the carbon concentration at the interface of the metallic carbide and the metal particle, C_B, can be expressed according to first-order kinetics,

$$\frac{dC_B}{dt} = k_B(C_S - C_B), \tag{1}$$

where the parameter k_B represents the coefficient of segregation-diffusion of the surface metallic carbide. It depends on the diffusivity of the carbon through the surface carbide, the carbide phase thickness, and the exposed surface area of this carbide. C_S represents the carbon surface concentration generated from the fed hydrocarbon decomposition (see Fig. 5). This parameter is mainly affected by the gas composition, pressure, and temperature during reaction. It will also vary with the remnant surface activity of the metal particles in the catalyst,

$$C_S = C_{S_0} a, \tag{2}$$

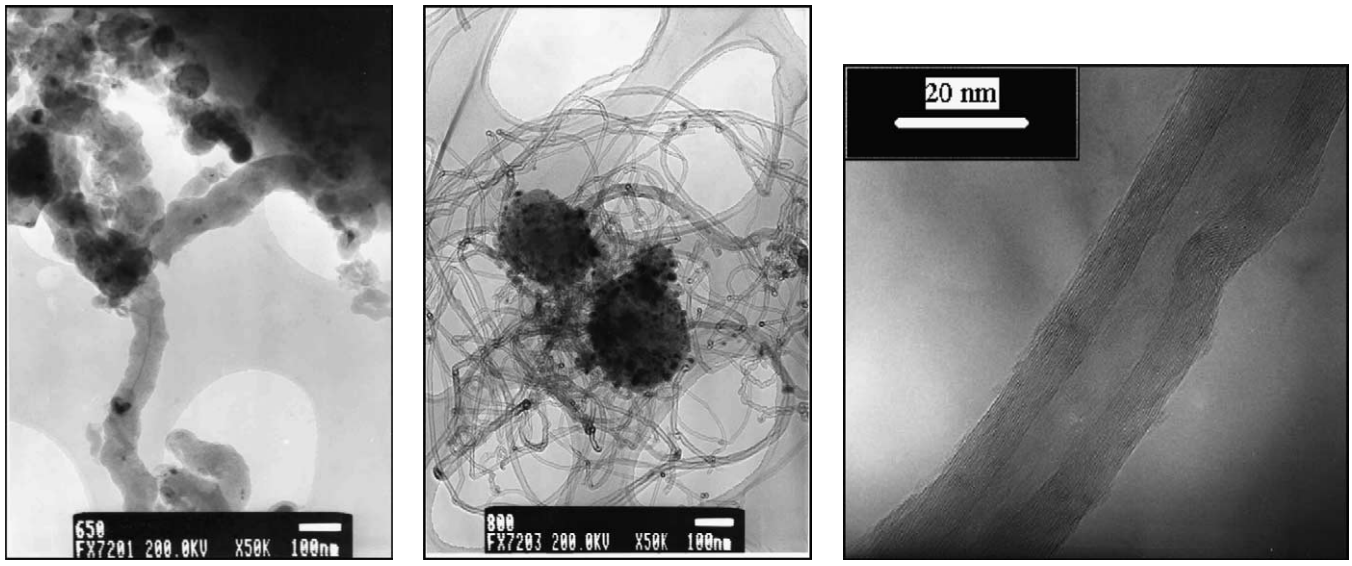

(a) (b) (c)

Fig. 4. TEM images of carbonaceous products at different temperatures: (a) CNFs obtained at 650 °C, (b) CNTs obtained at 800 °C, (c) HRTEM image of a CNT synthesized at 800 °C.

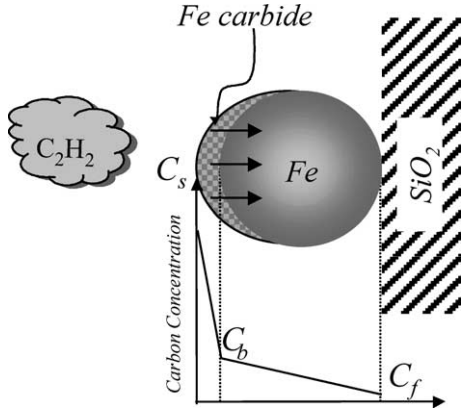

Fig. 5. Scheme with some parameters involved in the reaction kinetics of the growth mechanism of CNTs.

where C_{S_0} is the carbon concentration at the gas side of the metallic particles when the catalyst is not deactivated.

This model also considers that the catalyst can be deactivated by the formation of encapsulating coke. This coke can be partially removed from the catalyst surface by gasification with the hydrogen present in the reaction atmosphere. Consequently, the rate of catalyst deactivation is expressed as [31,32]

$$-\frac{da}{dt} = k_d a - k_r(1-a) = k_G(a - a_S), \tag{3}$$

where k_d and k_r are the deactivation and regeneration kinetic constants, respectively. For a given catalyst, both kinetic parameters are a function of the operating conditions, namely temperature and gas composition. The catalyst residual activity, a_S, and the parameter k_G, dependent on k_d and k_r, are expressed as follows:

$$a_S = k_r/(k_d + k_r), \qquad k_G = k_d + k_r. \tag{4}$$

The evolution in time of the surface carbon concentration is deduced from Eqs. (2) and (3):

$$C_S = C_{S_0}\big(a_S + (1 - a_S)\exp(-k_G t)\big). \tag{5}$$

The carbon formation (CNT) rate can be expressed as a function of the gradient of carbon concentration across the metallic particle, once the surface carbide has been produced,

$$r_C = k_C(C_B - C_F) \approx k_C C_B, \tag{6}$$

where C_B is the carbon concentration at the interface of the surface carbide and the metal particle and C_F is the carbon concentration generated after diffusion through the metal particle. It can be supposed that C_F is low, and so, its value is negligible with respect to C_B. The effective carbon transfer coefficient, k_C, depends on several factors such as the carbon diffusion coefficient, the average size of the metallic particles, and the exposed metallic surface area of the catalyst.

The evolution of carbon concentration in the interface carbide-metal particle, C_B, is deduced from Eqs. (1) and (5):

$$C_B(t) = C_{S_0}\big[a_S + k_G\alpha\exp(-k_G t) - k_B\beta\exp(-k_B t)\big]. \tag{7}$$

The terms α and β are given by

$$\alpha = k_B(1 - a_S)/k_G(k_B - k_G), \tag{8}$$

$$\beta = (k_B - k_G a_S)/k_B(k_B - k_G). \tag{9}$$

From Eqs. (6) and (7), the evolution of carbon formation rate in time can be expressed as (A. Monzón et al., in preparation)

$$r_C(t) = r_{C_0}\big[a_S + k_G\alpha\exp(-k_G t) - k_B\beta\exp(-k_B t)\big], \tag{10}$$

where the term r_{C_0} represents the maximum rate of CNT formation that can be attained in the absence of deactivation (A. Monzón et al., in preparation):

$$r_{C_0} = k_C C_{S_0}. \tag{11}$$

Finally the evolution of the carbon content accumulated on the catalyst, equivalent to CNTs production, can be calculated as

$$m_C(t) = \int r_C(t)\,dt. \tag{12}$$

The integration of Eq. (10) gives the following expression:

$$m_C(t) = r_{C_0}\big[a_S t + \alpha\big(1-\exp(-k_G t)\big) - \beta\big(1-\exp(-k_B t)\big)\big]. \tag{13}$$

In the case that the catalyst does not suffer deactivation, the above expression is simplified to

$$m_C(t) = r_{C_0}\left[t - \frac{1}{k_B}\big(1-\exp(-k_B t)\big)\right]. \tag{14}$$

Eq. (13) allows the prediction of the carbon content evolution over the catalyst as a function of the operating conditions. All the parameters of this kinetic model, r_{C_0}, k_B, k_d, and k_r, have a real physical meaning and show the great influence of the catalyst properties and the operating conditions on the CNT formation rate.

As discussed before, in Fig. 3, at low operating temperatures (600–675 °C) catalyst deactivation was observed and therefore, a decrease in the rate of CNT formation. On the contrary, at higher temperatures (700–800 °C) the catalyst did not seem to suffer deactivation and the reaction rate was constant, as observed in the high linearity of CNT growth curves in Fig. 3a. In Fig. 6 is seen the influence of reaction temperature on the determined kinetic parameters. Their evolution also points to the existence of both zones as discussed above. In Fig. 6b the temperature influence is just reflected in the parameters k_B and r_{C_0}, because the catalyst does not suffer deactivation and then we can admit that $k_d = k_r = 0$.

The proposed kinetic model explains perfectly well the experimental results: at low temperatures the catalyst suffers deactivation [Eq. (13)], although initially the carbon deposition rate has a high value, and at higher temperatures, the catalyst does not suffer deactivation [Eq. (14)], and initially the carbon deposition rate has a low value.

This behavior obviously should be related to the distinct morphology of the carbonaceous products isolated in both zones. At low temperatures the presence of amorphous materials was found (see Fig. 4a), and at high temperatures the products showed a higher graphitization degree, mainly carbon nanotubes (see Figs. 4b and 4c). These results seem to be logical if we think that at higher temperatures the formation of thermodynamically stable structures, like graphene layers, which constitute the basic structure of carbon nanotubes is favored. This will also explain why at low temperatures,

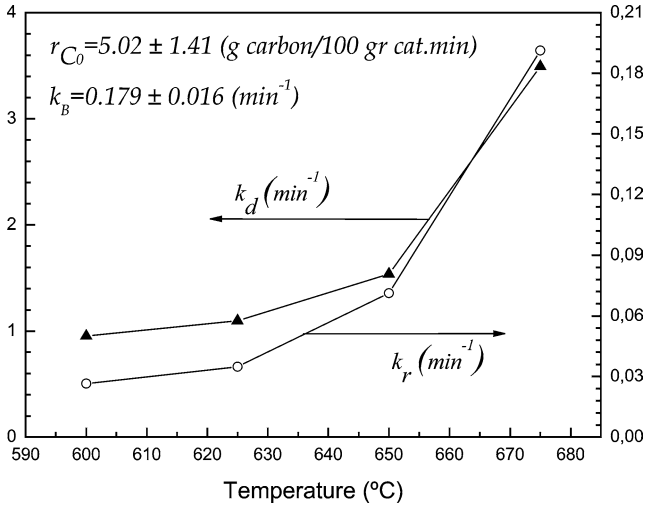

(a)

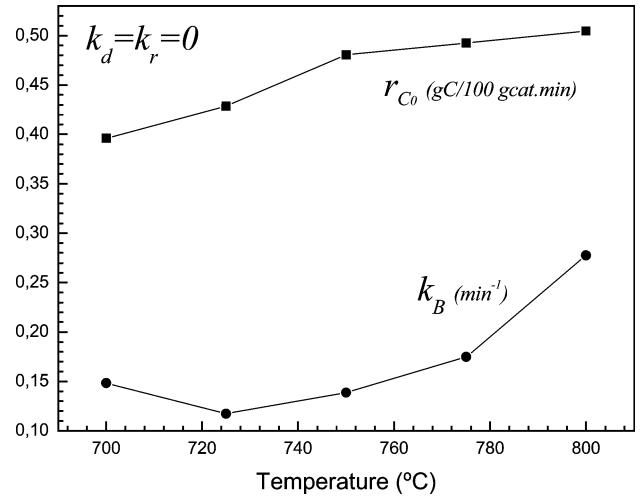

(b)

Fig. 6. Influence of reaction temperature on the kinetic parameters: (a) evolution of k_d and k_r at low temperatures, (b) evolution of r_{C_0} and k_B at high temperatures.

and low times, the r_{C_0} values are higher than at high temperatures, because in reality we are speaking about different carbonaceous materials.

In Figs. 7a and 7b are shown the Arrhenius-type plots for the kinetic parameters according to the following expressions:

(i) Low temperature zone,

$$k_C = \text{constant}, \qquad k_B = \text{constant},$$
$$k_d = k_{d_m}\exp\left[-\frac{E_d}{R}\left(\frac{1}{T}-\frac{1}{T_m}\right)\right],$$
$$k_r = k_{r_m}\exp\left[-\frac{E_r}{R}\left(\frac{1}{T}-\frac{1}{T_m}\right)\right]; \tag{15}$$

(ii) High temperature zone,

$$k_d = 0, \qquad k_r = 0,$$

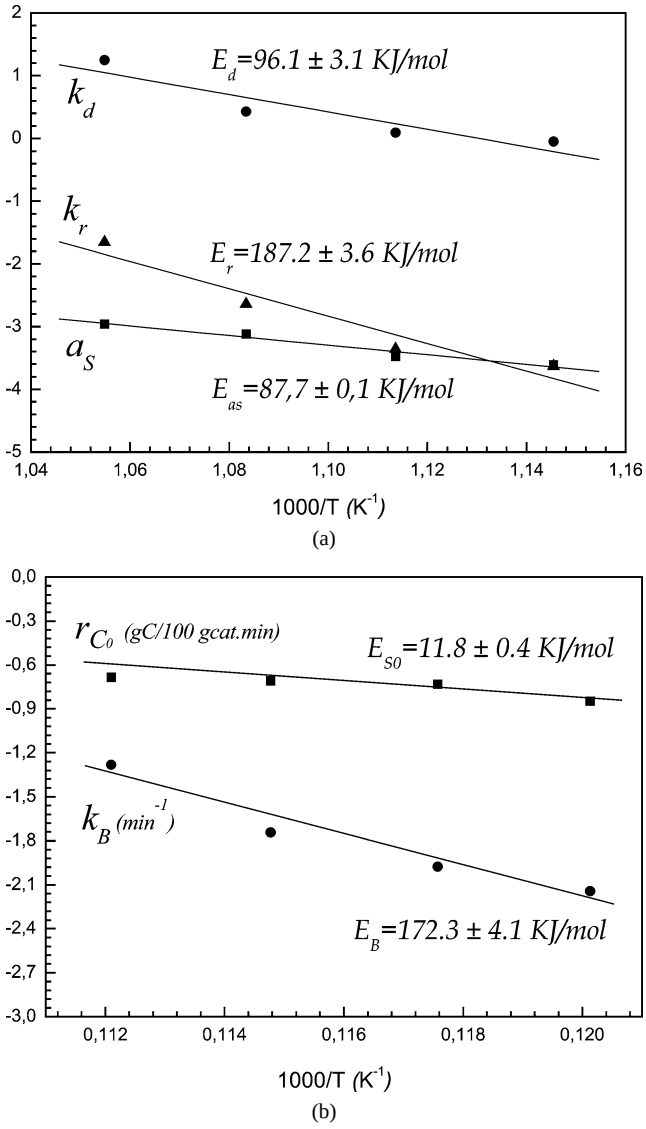

Fig. 7. Arrhenius-type plots for the kinetic parameters calculated at low (a) (< 700 °C) and high (b) (> 700 °C) temperatures.

$$r_{C_0} = A_{C_{0m}} \exp\left[-\frac{E_{CS}}{R}\left(\frac{1}{T}-\frac{1}{T_m}\right)\right],$$
$$k_B = A_{B_m} \exp\left[-\frac{E_B}{R}\left(\frac{1}{T}-\frac{1}{T_m}\right)\right]. \quad (16)$$

The values of the preexponential factors and the activation energies are calculated by multivariable nonlinear regression. According Eqs. (15) and (16), the kinetic parameters were reparametrized (see Tables 1 and 2) using as reference temperatures $T_m = 898$ and 1035.5 K.

In Table 1 it can be observed that the activation energy of the regeneration step, E_r, is higher than that of the deactivation stage, E_d, explaining why the residual activity of the catalyst increases with the temperature. The calculated value obtained for the activation energy of the regeneration step, E_r, was 187.2 kJ/mol (∼ 45 kcal/mol). Bartholomew reported an activation energy of 31 kcal/mol, calculated with

Table 1
Calculated values of the kinetic parameters obtained at low temperatures [Eq. (15); reparametrization temperature, $T_m = 898$ K]

Parameter	
r_{C_0} (min^{-1})	5.020 ± 1.414
k_B (min^{-1})	0.1789 ± 0.0158
k_{d_m} (min^{-1})	1.171 ± 0.325
E_d (J/mol)	96098 ± 3106
k_{r_m} (min^{-1})	0.0392 ± 0.0010
E_r (J/mol)	187182 ± 3649

Table 2
Calculated values of the kinetic parameters obtained at high temperatures [Eq. (16); reparametrization temperature, $T_m = 1035.5$ K]

Parameter	
A_{C_0m} (min^{-1})	0.4772 ± 0.0007
E_{CS} (J/mol)	11780 ± 353
A_{B_m} (min^{-1})	0.1829 ± 0.0033
E_B (J/mol)	172279 ± 4052

only two points, for the hydrogenation of what he named C_β [33]. This kind of carbon, C_β, was described as polymeric or graphitic carbon films encapsulating the metal surfaces, and could be related to the regeneration of the encapsulating coke we noted above. In Fig. 7a it can also be observed that the residual activity, a_S, follows an Arrhenius dependence with an apparent activation energy of 87.7 kJ/mol. This value is approximately the difference between E_d and E_r values deduced by substituting Eq. (15) in Eq. (4).

At low reaction temperatures (see Table 1) the value of r_{C_0} is almost 30 times higher than k_B, indicating that the diffusion step through the metallic particles is higher than the segregation of the surface metallic carbide. However, at high temperatures (see Table 2), r_{C_0} is only 2.6 times higher than k_B. In addition, at high temperatures the apparent activation energy of the parameter r_{C_0}, E_{CS}, is very low, 11.8 kJ/mol. Under these conditions, the reaction temperature mainly affects the carbide-segregation step, which showed an apparent activation energy of 172.3 kJ/mol (∼ 40 kcal/mol). This value is in concordance with the theoretical value (35 kcal/mol) for carbon diffusion through γ-Fe as reported in [14].

In Figs. 8 and 9 the influence of hydrogen and acetylene partial pressure on equation kinetic parameters is presented. As suggested in the analysis of Fig. 1A, it was assumed that the catalyst did not suffer deactivation with the variation of P_{H_2}, and therefore, Eq. (14) can be used to calculate the kinetic parameters. In Fig. 8 we can observe that the P_{H_2} does not seem to affect the value of parameter k_B; however, the value of r_{C_0} reaches a maximum at P_{H_2} of 7%, corroborating the observations made from Fig. 1A and the theoretical explanations exposed above.

In Fig. 9 the influence of $P_{C_2H_2}$ on the kinetic parameters is presented. An approximately first-order dependence between r_{C_0} and k_d with $P_{C_2H_2}$ is seen, as already observed

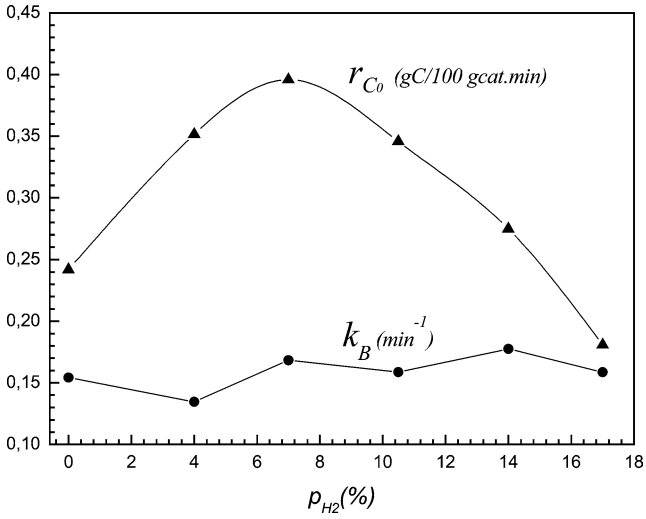

Fig. 8. Influence of P_{H_2} on the kinetic parameters of Eq. (14) (no deactivation of the catalyst).

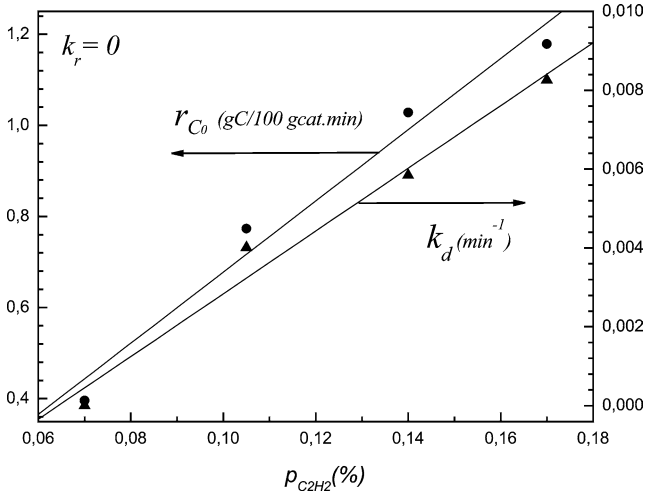

Fig. 9. Influence of $P_{C_2H_2}$ on the kinetic parameters of Eq. (13) (partial deactivation of the catalyst).

in Fig. 1B. The value of k_r was taken equal to zero and the coefficient of segregation-diffusion of the surface metallic carbide, k_B, was calculated and showed small variations with $P_{C_2H_2}$. The average value of k_B calculated in these experiments was 0.1697 ± 0.0123 (min^{-1}). These results predict that if we increase acetylene concentration, the deactivation constant, k_d, and the carbon concentration in the surface, C_{S_0}, are increased too [see Eq. (5)]. This explains the curvature of the graphics at high acetylene concentration in Fig. 1B, because of the notorious deactivation effect.

In conclusion it was found that both hydrogen and acetylene concentration variations do not affect the transference coefficient values, and mainly affect C_{S_0}, and so, r_{C_0} [Eq. (11)].

Nevertheless, to be completely sure about the parameter dependence with size of the catalytic metal particle, it would be necessary to test a series of experiments with different catalysts and different metal particle sizes. This way it would be possible to study carefully the real carbon diffusion through the catalyst under reaction conditions. These results could be of great importance in future studies of CNT growth with different catalysts and conditions. We would be able to select the proper conditions for the synthesis of CNTs in high yield with predetermined characteristics, and consider future applications of this novel material.

4. Conclusions

We have reported how reaction conditions such as P_{H_2}, $P_{C_2H_2}$ or reaction temperature can determine the final characteristics of the carbon deposits isolated after acetylene decomposition over an iron-supported catalyst. By variation of hydrogen and acetylene partial pressures we observed that the highest CNTs yield was obtained with a ratio 1:1 for H_2:C_2H_2. Furthermore, we observed a great influence of the temperature on this reaction in the thermogravimetric data as well as in TEM images. CNT yield and graphitization degree seemed to be linearly dependent on the reaction temperature. With the proposed kinetic model it is possible to describe the evolution of the CNT growth as a function of two diffusion parameters, r_{C_0} and k_B, and two deactivation parameters, k_d and k_r. The proposed mathematical equations are based on the theoretical diffusion-precipitation mechanism proposed in the bibliography.

Acknowledgments

The authors acknowledge financial support of DGI-MCYT, Madrid, Spain (Projects MAT2002-04189-CO2-O2, MAT2000-0043-P4-03, and PPQ2001-2479). We are also grateful to the Microscopy Centre “Luis Bru,” in the Complutense University at Madrid, for TEM and HRTEM studies. M.P.C. thanks the MECyD for a scholarship grant.

References

[1] J.L. Figuereido, C.A. Bernardo, R.T.K. Baker, K.J. Hüttinger (Eds.), Carbon Fibers Filaments and Composites, in: NATO ASI Ser. Ser. E, vol. 177, 1990, p. 405.
[2] A.J.H.M. Kock, P.K. de Bokx, E. Boellaard, W. Klop, J.W. Geus, J. Catal. 96 (1985) 454.
[3] K.P. de Jong, J.W. Geus, Catal. Rev.-Sci. Eng. 42 (2000) 481.
[4] S. Ijima, Nature 354 (1991) 56.
[5] P.M. Ajayan, Chem. Rev. 99 (1999) 1797.
[6] H. Dai, Surf. Sci. 500 (2002) 218.
[7] M. Pérez-Cabero, I. Rodríguez-Ramos, A. Guerrero-Ruíz, J. Catal. 215 (2003) 305.
[8] T.W. Ebbesen, P.M. Ajayan, Nature 358 (1992) 220.
[9] T. Guo, P. Nikolaev, A. Then, D.T. Colbert, R.E. Smalley, Chem. Phys. Lett. 243 (1995) 49.
[10] S. Amelinckx, X.B. Zhang, D. Bernaerts, X.F. Zhang, V. Joanov, J.B. Nagy, Science 265 (1994) 635.
[11] A. Borgna, L. Balzano, J.E. Herrera, W.E. Alvarez, D.E. Resasco, J. Catal. 204 (2001) 129.

[12] C.J. Lee, J. Park, Y. Huh, J.Y. Lee, Chem. Phys. Lett. 343 (2001) 33.
[13] N.M. Rodríguez, J. Mater. Res. 8 (12) (1993) 3233.
[14] Y.T. Lee, N.S. Kim, J. Park, J.H. Han, Y.S. Choi, H. Ryu, H.J. Lee, Chem. Phys. Lett. 372 (2003) 853.
[15] N. Nagaraju, A. Fonseca, Z. Konya, J.B. Nagy, J. Mol. Catal. A: Chem. 181 (2002) 57.
[16] J.I. Villacampa, C. Royo, E. Romeo, J.A. Montoya, P. del Angel, A. Monzón, Appl. Catal. A 252 (2003) 363.
[17] C.A. Bernardo, L.S. Lobo, J. Catal. 37 (1975) 267.
[18] I. Alstrup, J. Catal. 109 (1988) 241.
[19] I. Alstrup, M.T. Tavares, J. Catal. 135 (1992) 147.
[20] I. Alstrup, M.T. Tavares, J. Catal. 139 (1993) 513.
[21] K. Hernadi, A. Fonseca, J.B. Nagy, A. Siska, I. Kiricsi, Appl. Catal. A 199 (2000) 245.
[22] R.T.K. Baker, P.S. Harris, R.B. Thomas, R.J. Waite, J. Catal. 30 (1973) 86.
[23] A.J.H.M. Kock, P.K. de Bokx, E. Boellaard, W. Klop, J.W. Geus, J. Catal. 96 (1985) 468.
[24] J.W. Snoeck, G.F. Froment, M. Fowles, J. Catal. 169 (1997) 240.
[25] S.H. Lee, E. Ruckenstein, J. Catal. 107 (1987) 23.
[26] A. Sacco Jr., P. Thacker, T.N. Chang, A.T.S. Chiang, J. Catal. 85 (1984) 224.
[27] P. Navarro-López, I. Rodríguez-Ramos, A. Guerrero-Ruíz, Carbon 41 (2003) 2509.
[28] R. Marangoni, P. Serp, R. Feurer, Y. Kihn, P. Kalck, C. Vahlas, Carbon 39 (2001) 443.
[29] G.A. Jablonski, F.W. Geurts, A. Sacco Jr., R.R. Biederman, Carbon 30 (1992) 87.
[30] R.G. Olsson, E.T. Turkdogan, Metal. Trans. 5 (1974) 21.
[31] J.C. Rodríguez, J.A. Peña, A. Monzón, R. Hughes, K. Li, Chem. Eng. J. 58 (1995) 7.
[32] A. Monzón, E. Romeo, A. Borgna, Chem. Eng. J. 94 (2003) 19.
[33] C.H. Bartholomew, Appl. Catal. A 212 (2001) 17.